This article has been published in: Clinical Oral Investigations Jul 3. doi: 10.1007/s00784-018-2548-1. [Epub ahead of print]

Authors: Manuel Toledano[1], Inmaculada Cabello[1], Estrella Osorio[1], Fátima S. Aguilera[1], Antonio Luis Medina-Castillo[2], Manuel Toledano-Osorio[1*], Raquel Osorio[1].

Title: Zn-containing polymer nanogels promote cervical dentin remineralization.

Institution: [1]University of Granada, Faculty of Dentistry, Dental Materials Section.
Colegio Máximo de Cartuja s/n
18071 – Granada - Spain.

[2]University of Granada, NanoMyP. Spin-Off Enterprise.
Edificio BIC-Granada. Av. Innovación 1.
18016 - Armilla, Granada, Spain.

*Corresponding author: Mr. Manuel Toledano-Osorio.
University of Granada, Faculty of Dentistry
Dental Materials Section
Colegio Máximo de Cartuja s/n
18071 – Granada - Spain.
Tel.: +34-958243788
Fax: +34-958240809
Email: mtoledano@correo.ugr.es

Acknowledgements

This work was supported by grants MINECO/FEDER MAT2014-52036-P and MINECO/FEDER MAT2017-85999-P. Authors do not have a financial relationship with the organization that sponsored the research.

Abstract

Objective: Nanogels designing for effective treatment of eroded cervical dentin lesions. *Materials and Methods:* Polymethylmetacrylate-based nanoparticles (NPs) were doxycycline (D), calcium or zinc loaded. They were applied on eroded cervical dentin. Treated surfaces were characterized morphologically by atomic force and scanning electron microscopy, mechanically probed by a nanoindenter to test nanohardness and Young modulus, and chemically analyzed by Raman spectroscopy at 24 h and 7 d of storage. Data were submitted to ANOVA and Student-Newman-Keuls multiple comparisons tests. *Results:* Dentin treated with Zn-NPs attained the highest nanomechanical properties, mineralization and crystallinity among groups. Nanoroughness was lower in Zn-treated surfaces in comparison to dentin treated with un-doped gels. Dentin treated with Ca-NPs created the minimal calcification at the surface and showed the lowest Young modulus at peritubular dentin. Intertubular dentin appeared remineralized. Dentinal tubules were empty in samples treated with D-NPs, partially occluded in cervical dentin treated with undoped NPs and Ca-NPs, and mineral covered when specimens were treated with Zn-NPs. *Conclusions:* Zn-loaded NPs permit functional remineralization of eroded cervical dentin. Based on the tested nanomechanical and chemical properties, Zn-based nanogels are suitable for dentin remineralization. *Clinical Relevance:* The ability of zinc-loaded nanogels to promote dentin mineralization may offer new strategies for regeneration of eroded cervical dentin and effective treatment of dentin hypersensitivity.

Keywords: remineralization, calcium, zinc, nanoparticles, cervical dentin.

Introduction

Non-carious cervical lesions are pathological processes characterized by loss of dental hard tissues near the cementoenamel junction, in absence of caries [1]. They are significant predisposing factors for dentin hypersensitivity (DH) [2], which is generated by an extracellular matrix demineralization producing dentinal tubules exposure. Dentin is a highly mineralized tissue whose mechanical properties play an indispensable role in maintaining the stress/strain tooth behavior. Dentin extracellular matrix is composed by carbonate rich and calcium deficient hydroxyapatite (HAp) crystallites [3], disposed at extrafibrillar and intrafibrillar compartments of the collagen fibers. Dentinal tubules are surrounded by intertubular dentin (ID), which consists of a collagen matrix reinforced by apatite crystals similar to those of peritubular dentin (PD) [4]. Erosion and chemical degradation represent the etiology of DH [5]. Erosion is a complex process where the initial dissolution of the mineral exposes the organic matrix leaving a layer of fully demineralized organic matrix [6]. Degradation of the dentin matrix occurs after it has become accessible by the removal of mineral, i.e. the dentin matrix cannot be degraded unless it is demineralized [7]. Tubules occlusion and dentin remineralization are considered two of the main objectives of DH treatment [8, 9].

New biomaterials should facilitate dentin remineralization [10, 11] focusing on promoting regenerative processes of the extracellular matrix through interactions with the host tissue to release dentin bioactive molecules [12]. Some resins, varnishes and remineralizing agents [9] have been proposed for DH treatment, but most of them do not promote functional remineralization, do not demonstrate enough compatibility [13], and their effects are often transitory [14]. In dentin treatment, demineralized dentin infiltration with polymeric nanoparticles (NPs) as calcium and phosphate sequestering materials has been proposed. Anionic carboxylate sequences (COO^-) are on the NPs surfaces, allowing their complexation to cationic ions or molecules [11].

Metalloproteinases (MMPs) are activated when pH is lowered, as it occurs during caries and erosion processes [6]. Zinc inhibits MMPs-mediated collagen degradation and favors dentin remineralization [15]. Biological apatite is calcium deficient, and contains substantial amounts of

carbonate. Carbonated apatite is a precursor of HAp, but when it is precipitated in the presence of zinc, there is an *in vitro* exchange between Zn^{2+} and Ca^{2+}, forming a substituted apatite compound [16]. Furthermore, zinc incorporation into NPs raises the potential for intrafibrillar remineralization at partially demineralized collagen matrices [15]. Doxycycline potentiates hard tissues regeneration in periodontal defects when locally administrated due to its anticollagenolytic effect [17].

The degree and the quality of the mineralization will affect the mechanical properties of dentin. Indeed, the extrafibrilar minerals act as a granular material that can withstand load, but in the absence of intrafibrilar mineralization. Intrafibrilar mineralization is the key factor for ensuring that collagen fibrils have the same high modulus of elasticity as occurs in natural biomineralized dentin [18]. Atomic force microscopy (AFM) assisted nano-indentation does represent a specific applied mean of testing mechanical properties of some materials or substrates [19]. Raman spectroscopy is an analytical technique able to measure the molecular composition of dentin containing information regarding chemical changes within the samples [20, 21]. The combination of biochemical data with atomic force microscopy (AFM) techniques appears to be a valuable tool for applying in dentin remineralization studies [22].

The aim of this study was to investigate the efficacy of different nanogels to remineralize eroded cervical dentin. Surface roughness, mechanical and chemical changes occurring after treating cervical dentin surfaces with four different NPs solutions were analyzed. The null hypothesis that was established is that no changes in surface profilometry, mechanical and chemical properties were produced at *in vitro* eroded cervical dentin surfaces after different NPs application.

Material and Methods

Nanoparticles production

PolymP-*n* Active nanoparticles (NPs) (NanoMyP, Granada, Spain) were fabricated trough polymerization precipitation [23]. NPs are composed by 2-hydroxyethyl methacrylate (backbone monomer), ethylene glycol dimethacrylate (cross-linker) and methacrylic acid

(functional monomer). Calcium-doped NPs (Ca-NPs) and Zinc-doped NPs (Zn-NPs) were produced. For zinc and calcium complexation 30 mg of NPs were immersed at room temperature, during 3 days under continuous shaking in 15 ml aqueous solutions of $ZnCl_2$ or $CaCl_2$ (containing zinc or calcium at 40 ppm at pH 6.5), in order to reach the adsorption equilibrium of metal ions. Then, the suspensions were centrifuged and the particles were separated from the supernatant. Attained ion complexation values are 0.96 ± 0.04 μg Ca/mg NPs and 2.15 ± 0.05 μg Zn/mg NPs [24]. A third group of NPs doped with doxycycline was introduced in the study. 30 mg of NPs were immersed in 18 ml of 40 mg/ml aqueous solution of doxycycline hyclate (Sigma Aldrich, ChemieGmbh, Riedstr, Germany), during 4 hours, under continuous shaking. Then, the suspensions were centrifuged and the particles were separated from the supernatant. Following this procedure, loading efficacy is 70%, incorporated doxycycline to NPs is 900 μg/mL (per mg of NPs). Four different nanogels were tested: 1) NPs (NPs), 2) NPs doped with Ca (Ca-NPs), 3) NPs doped with Zn (Zn-NPs), and 4) NPs doped with doxycycline hyclate (D-NPs).

Specimen preparation

15 sound, single-rooted teeth were obtained with informed consent from donors (18 to 25 yr of age), under a protocol approved by the Institution review board (405/CEIH/2017). Two dentin blocks from the buccal surface of each root, just below the cementodentinal junction were obtained by cutting with a diamond saw (Accutom-50 Struers, Copenhagen, Denmark) under copious water irrigation. The surfaces were polished through SiC abrasive papers from 800 up to 4000 grit followed by final polishing steps performed using diamond pastes through 1 μm down to 0.25 μm (Struers LaboPol-4; Struers GmbH, Hannover, Germany) (Fig. 1). Specimens were prescreened for tubule occlusion with AFM and those with occluded tubules were excluded [25].

Dentin samples were dipped into a citric acid solution (pH 3.8) for 1 min to ensure the patency of the dentinal tubules and remove the smear layer [25]. Dentin surfaces were washed and ultrasound treated for 10 min before NPs application. A phosphate buffered saline (PBS) suspension of NPs, Zn-NPs, Ca-NPs, D-NPs (10 mg/ml) or just a PBS solution were applied (30 s), in each of the five different experimental groups. Each block of the same treated teeth was stored in PBS at 37º C for 24 hours and 7 days.

Nanoindentation

An atomic force microscope (AFM-Nanoscope V, Digital Instruments, Veeco Metrology group, Santa Barbara, CA, USA) equipped with a Triboscope indentor system (Hysitron Inc., Minneapolis, MN, USA) and a Berkovich indenter (tip radius 20 nm) was employed in this study. For each subgroup, three slabs were tested. On each slab, five indentation lines were executed in five different mesio-distal positions along the dentin surface in a straight line. Indentations were performed with a load of 4000 nN and a time function of 10 s. The indenter was progressively (at a constant rate) pressed over the sample up to a peak load of 4000 μN. Specimens were scanned in a hydrated condition. To avoid dehydration a layer of ethylene glycol over the specimen surface was applied, preventing water evaporation during a typical 25-to-30-min scanning period [26]. The distance between each indentation was kept constant by adjusting the distance intervals in 5 (±1) μm steps [27]. Hardness (*Hi*) and modulus of elasticity (*Ei*) data were registered in GPa.

The load, *F*, was obtained as a function of the penetration depth, *h*, of the indenter in the sample. From the slope of these load-*vs*.-depth curves the nanoindentation modulus (Young modulus) could be obtained by application of different theoretical models [28, 29]. One of these is the Oliver-Pharr method, which is based on a continuum, isotropic, homogeneous elastic contact model to determine the reduced modulus, E_r. In this model the slope, *S*, of the unloading portion of the load-*vs*.-depth data is used to obtain E_r according to the following equation [29]:

$$S = \frac{dF}{dh} = \frac{2}{\sqrt{\pi}} E_r \sqrt{A}, \qquad (1)$$

where A is the projected contact area of the hardness impression of the indenter. Then, E_i of the sample is obtained through the following expression:

$$\frac{1}{E_r} = \frac{\left(1-\nu_{ind}^2\right)}{E_{ind}} + \frac{\left(1-\nu_i^2\right)}{E_i}, \qquad (2)$$

In this expression "*i*" subscript refers to the tested sample and "*ind*" subscript to the indenter. ν and *E* are the Poisson's ratio and the Young modulus, respectively. For hard materials, as dentin, usually, $E_{ind} >> E_i$ and, thus, the contribution of the indenter in equation (2) can be neglected. With regard to the nanohardness of the sample, *H*, it is defined as:

$$H = \frac{F_{\max}}{A},$$

Where F_{max} is the peak load. In this work, values of nanohardness and Young modulus were automatically calculated by using the software Triboscan Quasi version 8.4.2.0 (Hysitron, Inc).

Data were analyzed by two-way ANOVA and Student-Newman-Keuls multiple comparisons tests ($P < 0.05$).

AFM imaging and nanoroughness assessments

An atomic force microscope (AFM Nanoscope V, Digital Instruments, Veeco Metrology group, Santa Barbara, CA, USA) was employed in this study for topography analysis. The imaging process was undertaken inside a wet cell in a fully hydrated state, using the tapping mode, with a calibrated vertical-engaged piezo-scanner (Digital Instrument, Santa Barbara, CA, USA). A 10-nm-radius silicon nitride tip (Veeco) was attached to the end of an oscillating cantilever that came into intermittent contact with the surface at the lowest point of the oscillation. Changes in vertical position of the AFM tip at resonance frequencies near 330 kHz provided the height of the images registered as bright and dark regions. 10 x 10 μm digital images were recorded with a slow scan rate (0.1 Hz). For each image, 5 randomized boxes (2 x 2 μm) and (1 x 1 μm) were created to examine the ID and PD nanoroughness at 24 h and 7 d of storage. Nanoroughness (SRa, in nanometers) was measured with proprietary software (Nanoscope Software, version V7). Data were submitted to ANOVA and Student-Newman-Keuls multiple comparisons tests ($p<0.05$).

Raman spectroscopy

The same dentin surfaces were, then, submitted to Raman analysis using a dispersive Raman spectrometer/microscope (Horiba Scientific Xplora, Villeneuve d´Ascq, France). A 785-nm diode laser through a X100/0.90 NA air objective was employed. Raman signal was acquired using a 600-lines/mm grafting centered between 400 and 1700 cm^{-1}. Chemical mapping of the surfaces was performed. For each specimen two areas 12x12 μm of the surfaces at different sites were mapped using 0.5 μm spacing at X and Y axis (625 points per map). The output from a clustering algorithm was basically a statistical description of the cluster centroids with the number of components in each cluster. The biochemical content of each cluster was analyzed using the

average cluster spectra. The natural groups of components (or data) based on some similarity and the centroids of a group of data sets were found by the clustering algorithm once calculated by the software and the Hierarchical Cluster Analysis (HCA). The observed spectra were described at 400-1700 cm^{-1} with 10 complete overlapping Gaussian lines, suggesting homogeneous data for further calculations [30]. At this point, the mineral component of dentin was assessed after the analysis of the relative presence of mineral, *i.e*, phosphate (960 cm^{-1}) and carbonate (1070 cm^{-1}) peaks and areas, relative mineral concentration of phosphate (PO_4^{3-}) and carbonate (CO_3^{2-}) referred to phenyl (RMC_p and RMC_c, respectively). Additional peaks were measured at 954 cm^{-1}, 956 cm^{-1} and 963 cm^{-1} to analyze the calcification of the extracellular matrix, the additional substituted or amorphous-like apatite species and the stoichiometric hydroxyapatite (HAp), respectively [20,31,32]. Crystallinity was also assessed based on the full width at half maximum (FWHM) of the phosphate band at 960 cm^{-1}, $FWHM_P$ [32]. The organic component of dentin was analyzed examining normalization at 1003 cm^{-1}, crosslinking at 1030/1032.7 cm^{-1} (Pyridinium ring vibration), and at 1550 cm^{-1} [AGEs, (advance glycation end products)-pentosidine], Nature of collagen at the amide III, CH_2, amide I and proteoglycans peaks [20,32]

Field Emission Scanning Electron Microscopy (FESEM) and energy dispersive (SEM/EDX) analyses

Representative specimens of each group were fixed in a solution of 2.5% glutaraldehyde in 0.1 mol/L sodium cacodylate buffer for 24 h, rinsed three times in 0.1 mol/L sodium cacodylate buffer. Samples were placed in an apparatus for critical point drying (Leica EM CPD 300, Wien, Austria). They were, then, sputter-coated with carbon by means of a sputter-coating Nanotech Polaron-SEMPREP2 (Polaron Equipment Ltd., Watford, UK) and observed with a field emission scanning electron microscope (FESEM Gemini, Carl Zeiss, Oberkochen, Germany) at an accelerating voltage of 3 kV. Energy-dispersive analysis was performed in selected points using an X-ray detector system (EDX Inca 300, Oxford Instruments, Oxford, UK) attached to the FESEM.

Results

The nanomechanical properties (*Hi* and *Ei)* of the cervical dentin surfaces at PD and ID were influenced by the type of NPs applied ($P<0.05$) and by the storage time ($P<0.05$). Interactions between factors were also significant ($P<0.05$). Mean and SD of *Hi* and *Ei* are represented in Figure 2. The highest *Hi* and *Ei* were achieved after 7 d of storage, at PD and ID, in specimens treated with Zn-NPs (Fig. 2). The lowest *Hi* values were reached at 7 d time point at ID in untreated dentin specimens. The lowest *Ei* after 7 d of storage was attained in dentin treated with Ca-NPs at both PD and ID. Intertubular and peritubular cervical dentin, untreated, decreased their *Hi* after 7 d. Zn-NPs application after 7 d contributed to increase *Hi* at PD. *Ei* decreased at ID in untreated cervical dentin surfaces after 7 d, and also at PD when surfaces were untreated or Ca-NPs treated. Dentin surfaces treated with Zn-NPs increased their *Ei* after 7 d of storage (Figs. 2a, 2b).

AFM images of untreated and Zn-NPs treated dentin surfaces, after 7 d storage are shown in Figure 3. The strong remineralization pattern of the dentin surface, and the staggered periodicity banding of collagen fibrils are shown at cervical dentin after Zn-NPs treatment. Nanoroughness (SRa) of dentin surfaces were influenced by the type of NPs applied ($P < 0.05$) and by storage time ($P < 0.05$); interactions between factors were also significant ($P < 0.05$). Mean and SD of nanoroughness are presented in Figure 2C. At ID and PD after 7 d, the lowest SRa values were obtained when the dentin surface was treated with D-NPs. Roughness at PD could not be measured after treating with Zn-NPs as only some tubules orifices were partially visible (Figs. 2c, 3b).

Results from Raman analysis are presented in Table 1 and Figure 5. Cervical dentin treated with Zn-NPs attained the highest degree of mineralization related to the phosphate (960 cm^{-1}) and carbonate (1070 cm^{-1}) at 7 d time point, as their peaks and areas showed the maximum values, among groups. The full width at half maximum ($FWHM_p$) of the phosphate (PO_4^{3-}) band at 961 cm^{-1}, was the lowest when Zn-NPs were applied, after 7 d of storage, showing the highest crystallinity among groups. This complied with the maximum height peak of the stoichiometric HAp band v_1 (963 cm^{-1}), ~743 cm^{-1} (Table 1). The highest amorphous-like apatite species shift band (956 cm^{-1}) occurred when dentin surfaces treated with Zn-NPs were assessed at 7 d. This

concurred with the major calcification (954 cm^{-1}) that was obtained among groups when Zn-NPs were applied on cervical dentin surfaces and measured at 7 d. Zn-NPs application generated the highest raise in collagen crosslinking, as the spectral bands at 1032 cm^{-1} (pyridinium) and 1550 cm^{-1} [advanced glycation-end-products (AGEs)-pentosidine)] reached the greatest intensities, at 7 d of storage. The molecular conformation of the collagen's polypeptide chains, amide-III (1246-1270 cm^{-1}), amide-I (1655-1667 cm^{-1}) and CH_2 (1450 cm^{-1}) also attained highest peaks in dentin treated with Zn-NPs, at 7 d time point.

FESEM images of the five different groups are shown in Figure 4. Peritubular and intertubular dentin appeared mineralized in specimens treated with NPs (Fig. 4b), D-NPs (Fig. 4c) and Ca-NPs (Fig. 4d), at 7 d storage. Dentinal tubules were empty in samples treated with D-NPs, partially occluded in cervical dentin treated with undoped NPs and Ca-NPs, and mineral covered when specimens were treated with Zn-NPs (Fig. 4e). Remineralized NPs were observed at the entrance of tubules in dentin treated with undoped NPs (Fig. 4b), Ca-NPs (Fig. 4d), and on the peritubular dentin and the tubular walls of dentin treated with D-NPs (Fig. 4c).

Discussion

The presence of zinc on NPs assures nanomechanical improvement and remineralization of cervical dentin with new crystalline HAp formation; however, non-crystalline amorphous-like apatite species were also encountered.

The general improvement of both *Ei* (equation 2) and *Hi* (equation 3) at the cervical dentin surface when Zn-NPs were applied and assessed after 7 d of storage (Figs. 2a, 2b), may be correlated, in the present research, with a remineralizing effect [15]. This result was linked to mineral precipitation (Ca, P and Zn) within the demineralized organic matrix [33]. It has been previously stated that nanomechanical properties recovery at the dentin substrate is only produced if functional and interfibrillar remineralization occurred [18], [34]. After 7 d of study, both Zn-NPs and D-NPs applied on cervical dentin showed the lowest nano-roughness values among groups (Fig. 2c). A decrease in roughness is associated to mineral maturation and it is a sight of intrafibrillar remineralization [35].

FESEM corroborated the presence of new mineral formation at cervical dentin surfaces after applying D-NPs (Fig. 4c) and Zn-NPs for 7 d (Fig. 4e), but the pattern of mineral precipitation differed between them. A consistent and continuous layer of mineral covered the dentin surface in both groups, but tubules remained open after the storage in the specimens treated with D-NPs or with un-doped NPs (Fig. 4b). There are long-lasting mineral precipitates at cervical dentin treated with Zn-NPs and also into the dentinal tubules (Fig 4e). It may also act as a mechanical barrier to the clinical erosive challenge [7]. Dentin hypersensitivity (DH) is clinically described as a non-spontaneous, localized, intense pain of short duration that ceases when stimuli are removed [36]. Erosion has been considered the main etiological factor for DH, because it is capable of opening and enlarging the dentin tubules [37]. Open dentinal tubules allow fluid flow through the tubules, which results in pressure changes that excite the nerve ending in the dental pulp [38]. The occlusion of dentinal tubules, therefore, is considered one of the main objectives of DH therapy [9, 10]. As tubules occlusion is mandatory for DH treatment [8, 9] then, the use of un-doped NPs and D-NPs is not indicated for this goal. On the other hand, Ca-NPs provoked the filling of dental tubules with nucleated minerals after 7 d of storage (Fig. 4d). The lowest mechanical properties, specifically the Young modulus at peritubular dentin (Fig. 2b), which denotes poor functional remineralization, discourages its indication for this purpose, and Zn-NPs are preferred.

After Raman analysis, cervical dentin remineralization was confirmed [20] (Table 1). HCA Raman images (clusters) (Fig. 5d) and results (centroids) (Fig. 5f) achieved at the dentin surface of specimens treated with Zn-NPs after 7 d of storage showed a generalized increase of the phosphate peak at the three distinguishable centroids (HCA_1, HCA_2 and HCA_3) (Fig. 5f) in comparison with the untreated samples at 7 d of storage time point (Fig. 5e). This indicates mineral gain. It is noteworthy that the increase of phosphate peak is accompanied by low RMC_p values. This finding is because RMC_p is a relative value (calculated as ratio between the phosphate peak and phenyl peak intensities); after Zn-NPS application intensity of the phenyl group reached the highest value (24.57 cm^{-1}), and as a consequence the ratio dropped. Moreover, Zn has demonstrated to inhibit MMPs and improve the crosslinking of the collagen (42). The presence

of a prominent carbonate band around 1070 cm^{-1} correlated with the increased degree of carbonate substitution in the lattice structure of apatite [39], and match with the narrowing full-width half-maximum ($FWHM_p$) of the phosphate v_1 peak (961 cm^{-1}), after treating the dentin surfaces with Zn-NPs (Table 1). $FWHM_p$ reflects a broad augmentation of crystallographic maturity, crystallinity, in minerals, at the surface [40], and it has been evidenced at Figs. 5e and 5f. The increase in crystallinity (*i.e.*, crystallographic maturity) at 961 cm^{-1} suggested the presence of hydroxyapatite crystals exhibiting a relative low degree of imperfections and substitutions [41]. This high crystallinity became associated to: *i)* the major phosphate v_1 vibration, at 963 cm^{-1} [31] (Table 1) which corresponded to stoichiometric HAp, and activates dentin remodeling with increased maturity [31] (Table 1), and *ii)* a high value of the peak intensity at 956 cm^{-1} which indicates additional substituted or amorphous-like apatite species [31].

Ratios concerning the crosslinking of collagen reflected a movement toward high frequencies after treating the cervical dentin surface with Zn-NPs, at 7 d (Table 1). This shift denoted a general rise at 1032 (pyridinium) [42], and 1550 cm^{-1} (AGES-pentosidine) at the dentin surface (Table 1). Cross-linking agents may be used to improve remineralization by combined reinforcement of demineralized dentin collagen matrix and inhibition of MMPs [6]. The Raman intensities which evoke the nature and secondary structure of collagen *i.e.,* CH_2 (1450 cm^{-1}) and Ratio Amide I/A-III, are clearly higher at dentin treated with Zn-NPs, after 7 d of storage time than at the rest of the groups (Table 1). This increase indicates recovery [43], better organization, improved structural differences and collagen quality [39]. This also explains the low RMC_p values that attained after applying Zn-NPs at dentin (Table 1). Therefore, the null hypothesis must be rejected.

In the present work, proteoglycan increased when Zn-NPs were applied and Raman values were assessed after 7 d of storage time, in comparison with 24 h storage. In dentin treated with Zn-NPs, proteoglycans were also higher in intensity than in the rest of the groups (Table 1). Proteoglycans act as bonding agents between the collagen network and the HAp crystals [44]. MMP-3 can release small leucine-rich proteoglycans and small integrin-binding ligand N-linked glycoproteins from dentin. These proteins participate in dentin mineralization, and inmobilized

phosphorylated proteins induce mineral formation [6]. Erosion plus demineralization has been considered the main etiological factor for DH, because of the opening and enlarging of the dentin tubules [8]. In erosion, the most important role seems to be played by MMPs that reduces dentin loss [45]. Host enzyme MMPs have been demonstrated to degrade the exposed organic matrix [46]. Zinc strongly reduces MMPs mediated collagen degradation in partially demineralized dentin. A collagen protector effect, exerted trough binding at the collagen sensitive cleavage sites of MMPs, has been advocated, so MMPs will be able to act in the subsequent biomimetic and functional remineralization process [46]. On the other hand, dentin treated with Ca-NPs created the minimal calcification at the surface, as v_1 (954 cm^{-1}) attained the lowest peak among groups (Table 1). Ca^{++} ions scarcely contribute to functional remineralization of cervical dentin (Figs. 2a, 2b), and Ca-NPs promoted partial occlusion of dentinal tubules (Fig. 4d). Even more, Ca-NPs applied on eroded cervical dentin attained generally the lowest Raman peak heights of both phosphate and carbonate after 7 d of storage (Table 1). Besides, the shift bands corresponding to crosslinking and proteoglycans were also the lowest (Table 1).

This paper is, to the best of our knowledge, the only response provided to the question over if this demineralized organic matrix that was seen at the cervical dentin surface can be remineralized [6]. Zn-NPs based-nanogel has been proved as bioactive material, and these results are promising even if the studies so far have been limited to *in vitro* testing. Hence this research demonstrates that the nature and secondary structure of collagen improved after treating the dentin surface with Zn-NPs. Non-collagenous mineralization-promoting proteins or their analogues, (*i.e.*, NPs) did prove remineralization of partially demineralized cervical dentin. Relative to complementary experimental techniques that ultimately illustrate the clinical outcome of cervical dentin, High Resolution TEM (HRTEM), Scanning Transmission Electron Microscopy (STEM) and nano-DMA analysis should be incorporated into our methodology for future strategies of research.

Compliance with ethical standards

Conflict of Interest: Manuel Toledano declares that he has no conflict of interest. Inmaculada Cabello declares that she has no conflict of interest. Estrella Osorio declares that she has no conflict of interest. Fátima S. Aguilera declares that she has no conflict of interest. Antonio Luis Medina-Castillo declares that he has no conflict of interest. Manuel Toledano-Osorio declares that he has no conflict of interest. Raquel Osorio declares that she has no conflict of interest.

Funding: This study was funded by the Ministry of Economy and Competitiveness (MINECO) and European Regional Development Fund (FEDER), grant numbers MAT2014-52036-P and MAT2017-85999-P. Authors do not have a financial relationship with the organization that sponsored the research.

Ethical approval: All procedures performed in the present study, involving human participants, were in accordance with the ethical standards of the institutional research committee (405/CEIH/2017) and with the 1964 Helsinki Declaration and its later amendments or comparable ethical standards. This article does not contain any studies with animals performed by any of the authors.

Informed consent Informed consent was obtained from all individual participants included in the study.

References

[1] Bartlett DW, Shah P (2006) A critical review of non-carious cervical (wear) lesions and the role of abfraction, erosion, and abrasion. J Dent Res 85:306–312. doi: 101177/154405910608500405

[2] West N, Seong J, Davies M (2014) Dentine hypersensitivity. Monogr Oral Sci 25:108–122. doi:101159/000360749

[3] Marshall GW, Marshall SJ, Kinney JH, Balooch M (1997) The dentin substrate: structure and properties related to bonding. J Dent 25:441–458. doi:10.1016/S0300-5712(96)00065-6

[4] Kinney JH, Marshall SJ, Marshall GW (2003) The mechanical properties of human dentin: a critical review and re-evaluation of the dental literatura. Crit Rev Oral Biol 14:13–29

[5] Lussi A, Schlueter N, Rakhmatullina E, Ganss C (2011) Dental erosion--an overview with emphasis on chemical and histopathological aspects. Caries Res 45:2–12. doi: org/101159/000325915

[6] Buzalaf MA, Charone S, Tjäderhane L (2015) Role of host-derived proteinases in dentine caries and erosion. Caries Res 49:30–37. doi:101159/000380885

[7] Kato MT, Leite AL, Hannas AR, Buzalaf MA (2010) Gels containing MMP inhibitors prevent dental erosion in situ. J Dent Res 89:468-472. doi: 101177/0022034510363248

[8] Gandolfi MG, Iacono F, Pirani C, Prati C (2012) The use of calcium-silicate cements to reduce dentine permeability. Arch Oral Biol 57:1054–1061. doi:101016/jarchoralbio201202024

[9] Wang Z, Jiang T, Sauro S, Pashley DH, Toledano M, Osorio R, Liang S, Xing W, Sa Y, Wang, Y (2011) The dentine remineralization activity of a desensitizing bioactive glass-containing toothpaste: an in vitro study. Aust Dent J 56:372–381. doi:101111/j1834-7819201101361x

[10] Gandolfi MG, Taddei P, Siboni F, Modena E, De Stefano ED, Prati C (2011) Biomimetic remineralization of human dentin using promising innovative calcium-silicate hybrid "smart" materials. Dent Mater 27:1055–1069. doi:101016/jdental201107007

[11] Osorio R, Alfonso-Rodríguez CA, Medina-Castillo AL, Alaminos M, Toledano M (2016) Bioactive Polymeric Nanoparticles for Periodontal Therapy. PloS One 11: e0166217. doi:10.1371/journal.pone.0166217

[12] Smith AJ, Scheven BA, Takahashi Y, Ferracane JL, Shelton RM, Cooper PR (2012) Dentine as a bioactive extracellular matrix. Arch Oral Biol 57:109–121. doi:101016/jarchoralbio201107008

[13] Niu LN, Zhang W, Pashley DH, Breschi L, Mao J, Chen JH, Tay FR (2014) Biomimetic remineralization of dentin. Dent Mater 30:77–96. doi:101016/jdental201307013

[14] Cartwright RB (2014) Dentinal hypersensitivity: a narrative review. Community Dent Health 31:15–20. doi:10.1922/CDH_3287Cartwright06

[15] Toledano M, Osorio R, Osorio E, Medina-Castillo AL, Toledano-Osorio M, Aguilera FS, (2017) Ions-modified nanoparticles affect functional remineralization and energy dissipation through the resin-dentin interface. J Mech Behav Biomed Mater 68: 62–79. doi:101016/jjmbbm201701026

[16] Mayer I, Apfelbaum F, Featherstone JD (1994) Zinc ions in synthetic carbonated hydroxyapatites. Arch Oral Biol 39:87–90. doi:10.1016/0003-9969(94)90040-X

[17] Agarwal A, Bhattacharya HS, Srikanth G, Singh A (2013) Comparative evaluation of decalcified freeze dried bone allograft with and without local doxycycline in non-contained human periodontal infrabony defects. J Indian Soc Periodontol 17:490-494. doi: 10.4103/0972-124X.118322

[18] Balooch M, Habelitz S, Kinney JH, Marshall SJ, Marshall GW (2008) Mechanical properties of mineralized collagen fibrils as influenced by demineralization. J Struct Biol 162:404–410. doi:101016/jjsb200802010

[19] Poon B, Rittel D, Ravichandran G (2008) An analysis of nanoindentation in linearly elastic solids. Int J Solids Struct 45:6018–6033. doi: 101016/jijsolstr200807021

[20] Kunstar A, Leijten J, van Leuveren S, Hilderink J, Otto C, van Blitterswijk CA, Karperien M, van Apeldoorn AA (2012) Recognizing different tissues in human fetal femur cartilage by label-free Raman microspectroscopy. J Biomed Opt 17:116012. doi:101117/1JBO1711116012

[21] Toledano M, Aguilera FS, Osorio E, Cabello I, Toledano-Osorio M, Osorio R (2015) Self-etching zinc-doped adhesives improve the potential of caries-affected dentin to be functionally remineralized. Biointerphases 10:031002. doi:101116/14926442

[22] Wang L, Zhao Y, Mei L, Yu H, Muhammad I, Pan Y, Huang S (2017) Effect of application time of maleic acid on smear layer removal and mechanical properties of root canal dentin. Acta Odontol Scand 75:59–66. doi:101080/0001635720161248789

[23] Medina-Castillo AL, Fernandez-Sanchez JF, Segura-Carretero A, Fernandez-Gutierrez A (2010) Micrometer and submicrometer particles prepared by precipitation polymerization: Thermodynamic model and experimental evidence of the relation between flory's parameter and particle size. Macromolecules 43:5804–5813. doi:101021/ma100841c

[24] Osorio R, Cabello I, Medina-Castillo AL, Osorio E, Toledano M (2016) Zinc-modified nanopolymers improve the quality of resin-dentin bonded interfaces. Clin Oral Investig 20:2411-2420. doi:101007/s00784-016-1738-y

[25] Saeki K, Marshall GW, Gansky SA, Parkinson CR, Marshall SJ (2016) Strontium effects on root dentin tubule occlusion and nanomechanical properties. Dent Mater 32: 240–251. doi:10.1016/j.dental.2015.11.020

[26] Ryou H, Niu L.N., Dai L, Pucci CR, Arola DD, Pashley DH, Tay FR (2011) Effect of biomimetic remineralization on the dynamic nanomechanical properties of dentin hybrid layers. J Dent Res 90:1122–1128. doi:10.1177/0022034511414059

[27] Toledano M, Sauro S, Cabello I, Watson T, Osorio R (2013) A Zn-doped etch-and-rinse adhesive may improve the mechanical properties and the integrity at the bonded-dentin interface. Dent Mater 29:e142-152. doi:10.1016/j.dental.2013.04.024

[28] Han L, Grodzinsky AJ, Ortiz C (2011) Nanomechanics of the Cartilage Extracellular Matrix. Annu Rev Mater Res 41:133-168. doi:101146/annurev-matsci-062910-100431

[29] Oliver WC, Pharr GM (1992) An improved technique for determining hardness and elastic modulus using load and displacement sensing indentation experiments. J Mater Res 7:1564–1583. doi:101557/JMR19921564

[30] Ager JW, Nalla RK, Breeden, KL, Ritchie, RO (2005) Deep-ultraviolet Raman spectroscopy study of the effect of aging on human cortical bone. J Biomed Opt 10:034012. doi:101117/11924668

[31] Timlin JA, Carden A, Morris MD, Rajachar RM, Kohn DH (2000) Raman spectroscopic imaging markers for fatigue-related microdamage in bovine bone. Anal Chem 72: 2229–2236. doi:10.1021/ac9913560

[32] Toledano M, Osorio R, Osorio E, García-Godoy F, Toledano-Osorio M, Aguilera FS (2016) Advanced zinc-doped adhesives for high performance at the resin-carious dentin interface. J Mech Behav Biomed Mater 62:247-267. doi: 10.1016/j.jmbbm.2016.05.013

[33] McKee MD, Nakano Y, Masica DL, Gray JJ, Lemire I, Heft R, Whyte MP, Crine P, Millán JL (2011) Enzyme replacement therapy prevents dental defects in a model of hypophosphatasia. J Dent Res 90:470–476. doi:101177/0022034510393517

[34] Bertassoni LE, Habelitz S, Kinney JH, Marshall SJ, Marshall GW (2009) Biomechanical perspective on the remineralization of dentin. Caries Res 43:70–77. doi:101159/000201593

[35] Zurick KM, Qin C, Bernards MT (2013) Mineralization induction effects of osteopontin, bone sialoprotein, and dentin phosphoprotein on a biomimetic collagen substrate J Biomed Mater Res A 101:1571–1581. doi:101002/jbma34462

[36] Jena A, Shashirekha, G (2015) Comparison of efficacy of three different desensitizing agents for in-office relief of dentin hypersensitivity: A 4 weeks clinical study. J Conserv Dent 18:389–393. doi:104103/0972-0707164052

[37] Yoshizaki KT, Francisconi-Dos-Rios LF, Sobral MA, Aranha AC, Mendes FM, Scaramucci T (2017) Clinical features and factors associated with non-carious cervical lesions and dentin hypersensitivity. J Oral Rehabil 44:112–118. doi:101111/joor12469

[38] Lynch E, Brauer DS, Karpukhina N, Gillam DG, Hill RG (2012) Multi-component bioactive glasses of varying fluoride content for treating dentin hypersensitivity. Dent Mater 28:168–178. doi:101016/jdental201111021

[39] Salehi H, Terrer E, Panayotov I, Levallois B, Jacquot B, Tassery H, Cuisinier F (2013) Functional mapping of human sound and carious enamel and dentin with Raman spectroscopy. J Biophotonics 6:765–774. doi:101002/jbio201200095

[40] Schwartz AG, Pasteris JD, Genin GM, Daulton TL, Thomopoulos S (2012) Mineral distributions at the developing tendon enthesis. PloS One 7:e48630. doi:101371/journalpone0048630

[41] Wang C, Wang Y, Huffman NT, Cui C, Yao X, Midura S, Midura RJ, Gorski JP (2009) Confocal laser Raman microspectroscopy of biomineralization foci in UMR 106 osteoblastic cultures reveals temporally synchronized protein changes preceding and accompanying mineral crystal deposition. J Biol Chem 284:7100–7113. doi:101074/jbcM805898200

[42] Osorio R, Osorio E, Cabello I, Toledano M (2014) Zinc induces apatite and scholzite formation during dentin remineralization. Caries Res 48:276-290. doi: 10.1159/000356873

[43] Xu C, Wang Y (2012) Collagen cross linking increases its biodegradation resistance in wet dentin bonding. J Adhes Dent 14:11–18. doi:103290/jjada21494

[44] Bakland LK, Andreasen JO (2012) Will mineral trioxide aggregate replace calcium hydroxide in treating pulpal and periodontal healing complications subsequent to dental trauma? A review. Dent Traumatol 28:25–32. doi:101111/j1600-9657201101049x

[45] Hannas AR, Zarella BL, Charone S, Taioki V, Kato MT, Tjäderhane L, Buzalaf MAR (2014) Dentin erosion prevention by matrix metalloproteinase and cysteine cathepsin inhibition. Dent Mater 30:e133 - e134. doi:101016/jdental201408275

[46] Osorio R, Yamauti M, Osorio E, Román JS, Toledano M (2011) Zinc-doped dentin adhesive for collagen protection at the hybrid layer. Eur J Oral Sci 119:401–410. doi:101111/j1600-0722201100853x

Table 1. Raman intensities (in arbitrary units) of mineral and organic components at eroded cervical dentin surfaces.

Mineral components												
			Untreated dentin		NPs		D-NPs		Ca-NPs		Zn-NPs	
			24h	7d	24h	7d	24h	7d	24h	7d	24h	7d
Relative Presence of Mineral	Phosphate (961)	Peak	465.73	486.72	575.49	622.66	753.32	685.64	503.20	551.64	726.57	804.68
		Area	11600.8	12371.7	14597.9	15790.2	19098.4	17392.0	12760.7	13996.5	18425.2	20284.6
		RMC_P	23.55	30.01	25.58	24.18	38.14	34.70	30.37	33.66	35.35	32.75
	Carbonate (1070)	Peak	57.65	58.50	72.22	71.70	103.96	91.26	66.45	72.18	99.80	108.66
		Area	1940.45	1778.2	2390.7	2168.8	3439.1	3575.9	2603.6	2389.2	3612.7	3890.9
		RMC_C	2.91	3.61	3.21	2.78	5.26	4.62	4.01	4.40	4.84	4.42
Crystallinity ($FWHM_p$)			19.01	19.40	19.36	19.35	19.35	19.36	19.36	19.36	19.35	19.24
v1 (954)			370.88	371.00	430.36	465.13	544.30	490.94	415.69	428.61	509.50	548.62
v1 (956)			417.33	465.41	491.13	530.67	630.41	567.23	462.40	485.84	592.72	640.49
v1 (963)			429.51	420.31	555.51	554.08	665.49	614.94	457.92	519.22	654.36	743.21
Organic components												
Normalization	Phenyl (1003)		19.78	16.22	22.50	25.75	19.75	19.76	16.57	16.39	20.64	24.57
Crosslinking	Pyridinium (1032)		28.67	21.69	36.68	38.69	35.51	32.95	31.37	28.72	32.71	40.20
	AGEs-Pentosidine (1550)		6.39	7.20	5.14	4.98	9.40	7.98	5.31	6.04	9.85	9.29
Nature and secondary structure of collagen	A-III (1246-1270)		34.82	36.26	40.17	43.56	53.49	48.51	42.1	38.55	52.41	55.88
	CH_2 (1450)		22.48	22.86	25.26	27.06	31.77	28.58	27.11	24.42	31.61	33.97
	A-I (1655-1667)		4.45	5.24	3.98	4.72	11.05	10.59	6.44	6.16	12.02	11.22
	Proteoglycans (1062)		34.65	32.07	42.55	44.26	52.03	46.34	35.93	35.83	45.45	51.40

For the mineral components, the peaks values had been normalized to the basis intensity of the symmetric phosphate band, near 996 cm^{-1}. For the organic components, the peaks values had been normalized to the basis intensity of the Amide II band near 1510 cm^{-1}. Peaks positions are expressed in cm^{-1}. NPs: unloaded nanoparticles; D-NPs: doxycycline doped nanoparticles; Ca-NPs: Ca doped nanoparticles; Zn: Zn doped nanoparticles; RMC: Relative mineral concentration between mineral/Phenyl (1003 cm^{-1}); FWHM: Full-width half-maximum; A: amide; AGEs: advanced glycation end products.

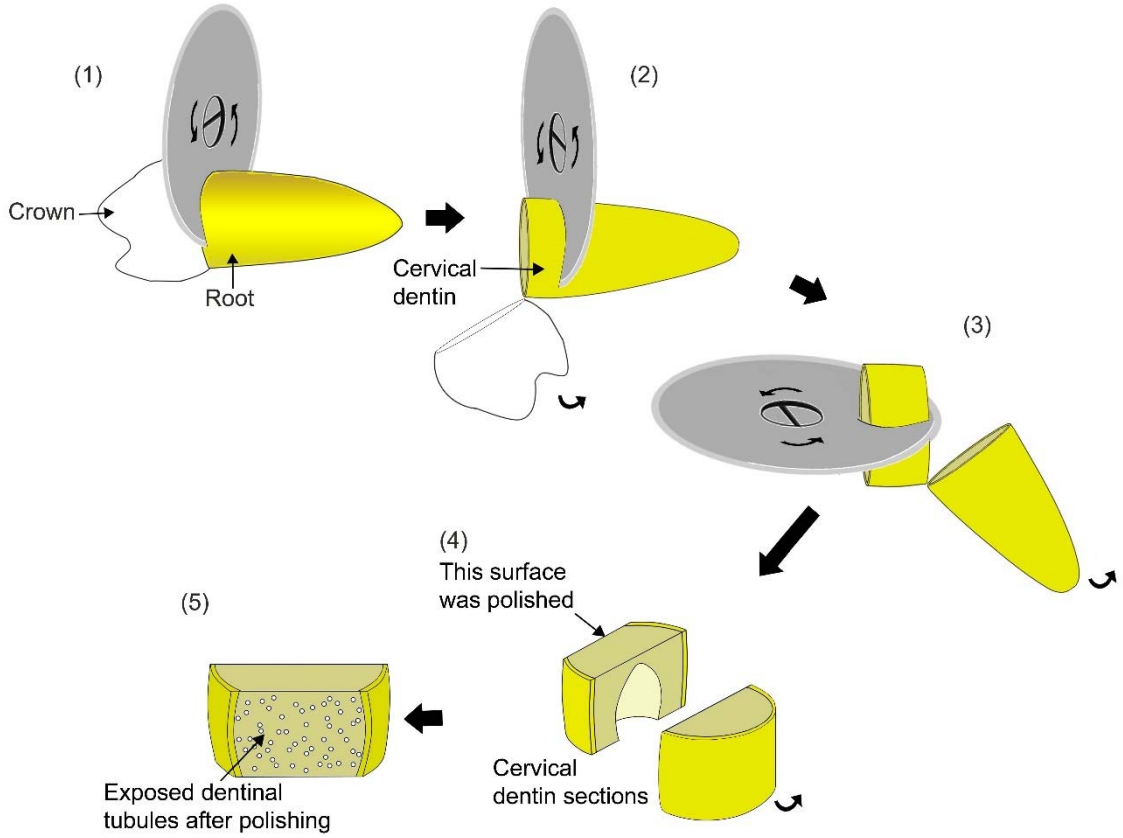

Fig 1 Schematic representation of specimen preparation. Tooth coronal section was discarded (1), a disc of cervical dentin was obtained (2), a longitudinal cut was also made to obtain two halves of the original specimen (3), two dentin blocks were prepared by cutting below the cementodentinal junction (4), surfaces were polished (5) to expose the cervical dentin

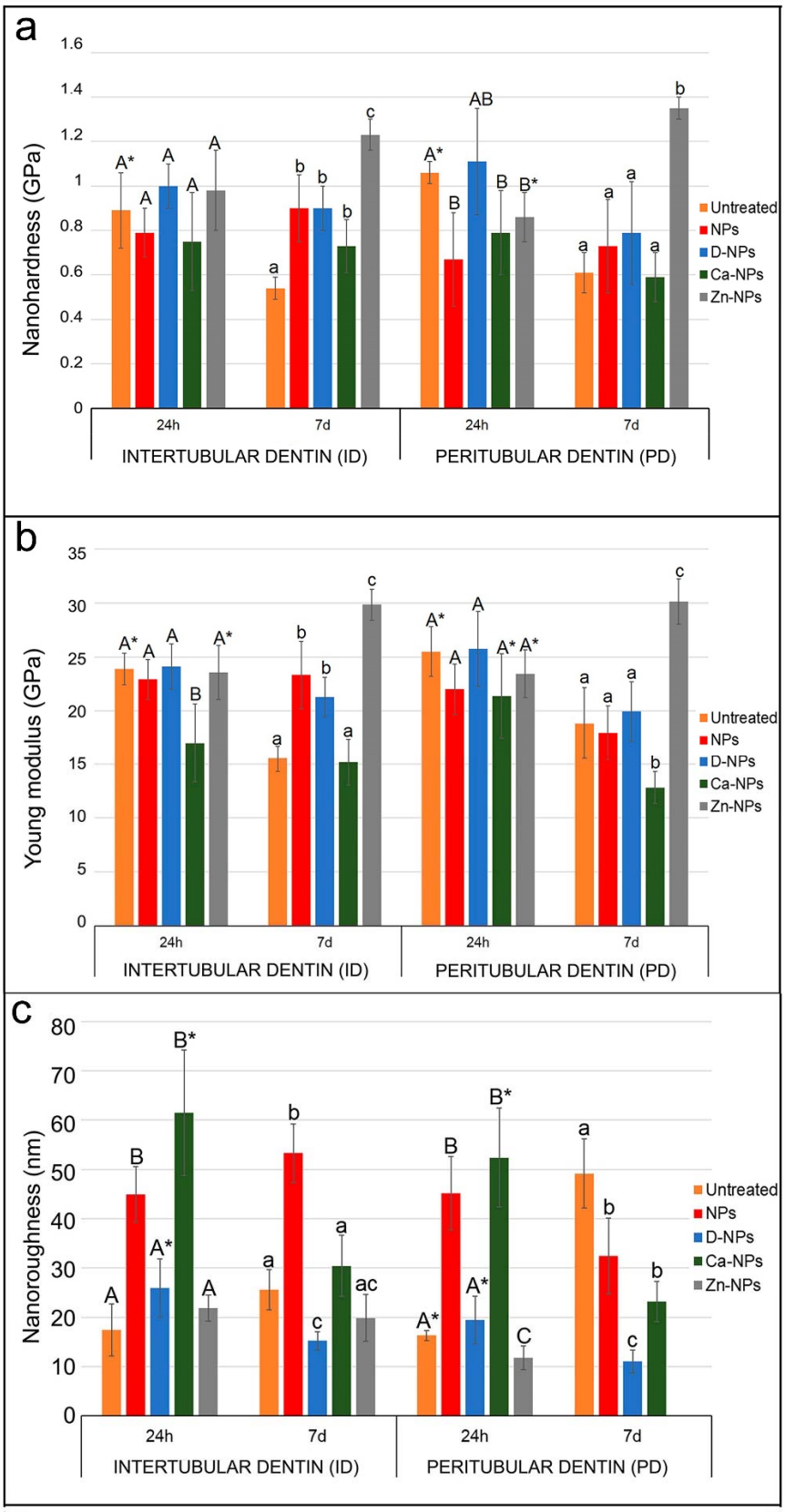

Fig 2 **a**, Mean and standard deviation of nanohardness values (*Hi*) (GPa) at eroded cervical dentin surfaces of the different experimental groups. **b**, Mean and standard deviation of Young modulus values (*Ei*) (GPa) at eroded cervical dentin surfaces of the different experimental groups. **c**, Mean and standard deviation of average surface nanoroughness values (SRa) (nm) at eroded cervical dentin surfaces of the different experimental groups. Same letter (capital for 24 h and lowercase

for 7 d) indicates no significant differences between treatment groups at the same dentin type. * indicates significant differences between the different storage periods in the same treatment group and dentin type. Abbreviations: NPs: unloaded nanoparticles; D-NPs: doxycycline doped nanoparticles; Ca-NPs: Ca doped nanoparticles; Zn-NPs: Zn doped nanoparticles

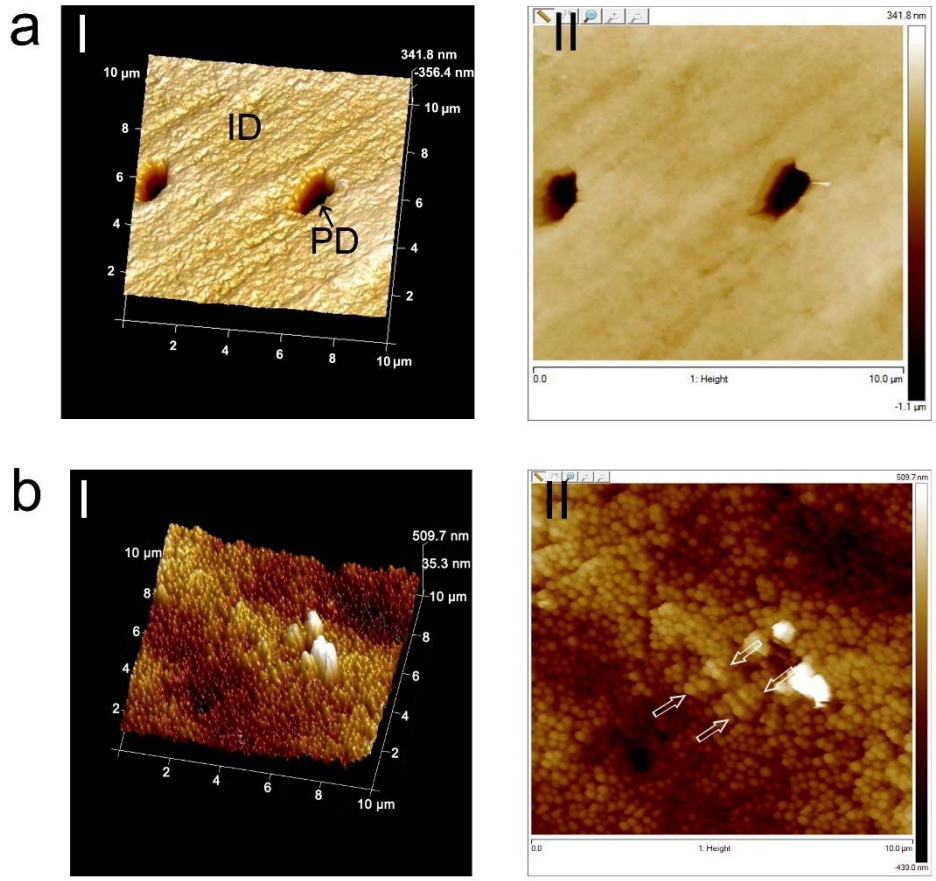

Fig 3 a, (I) 10 x 10 µm top-view and surface plot image of untreated cervical dentin at 7 d of storage. Opened dentinal tubules are observed. Peritubular (PD) and intertubular (ID) dentin appear well differentiated. (II) AFM phase image (10 x 10 µm) of this partially demineralized dentin surface. **b**, (I) 10 x 10 µm top-view and surface plot image of cervical after applying Zn-NPs, at 7 d of storage. The dentin surface is totally remineralized. (II) AFM phase image (10 x 10 µm) showing the wider bandwidth of the collagen fibrils and the staggered pattern of collagen fibrils (faced arrows)

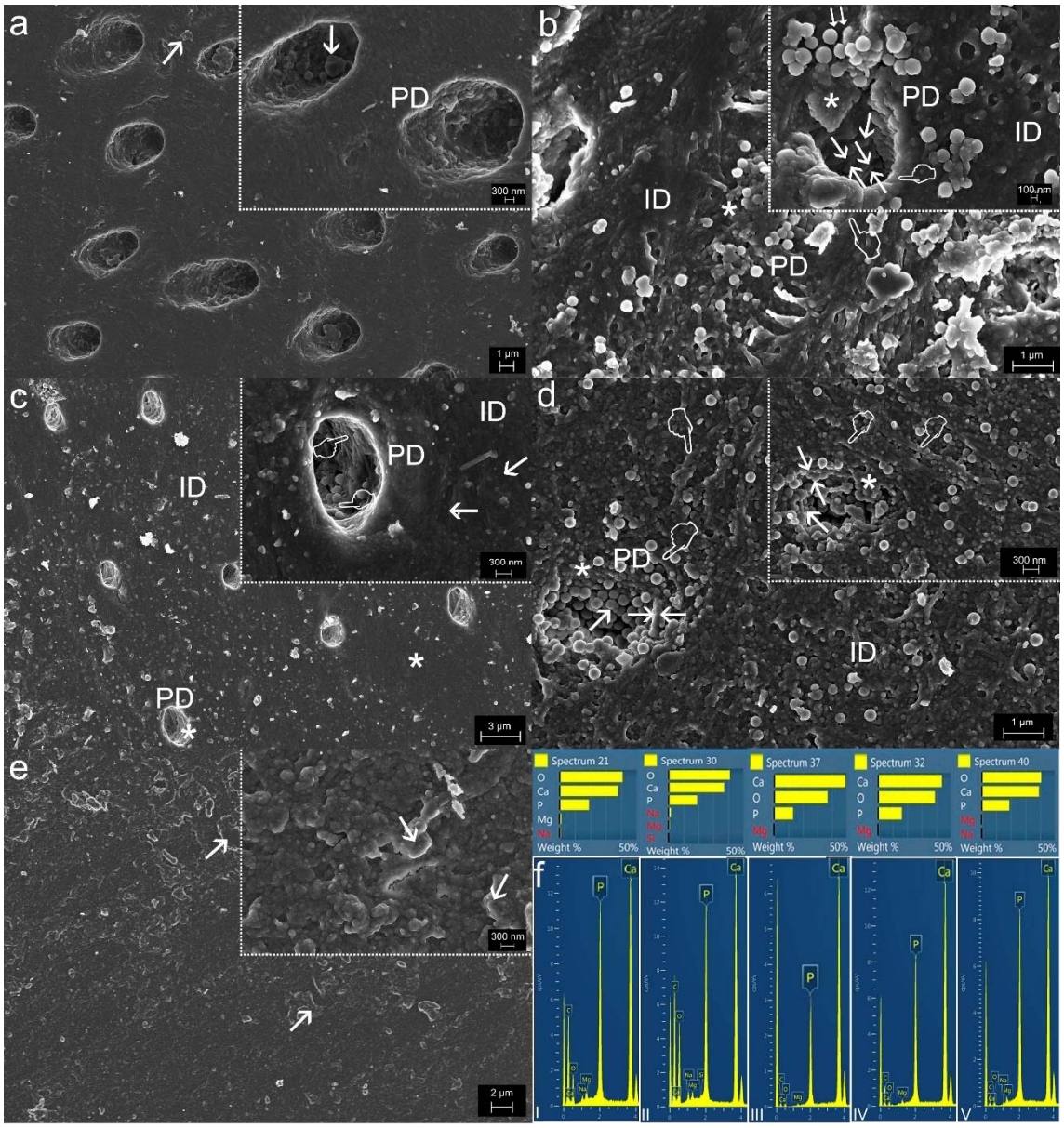

Fig 4 a, Field emission scanning electron microscopy (FESEM) image of untreated eroded cervical dentin, shown after 7 d of storage (scale bar: 1 µm). A few crystals or mineral deposits were occasionally encountered on both intertubular and peritubular dentin (arrows). Tubules appeared mineral free with a clear ring of peritubular dentin (PD) (inset scale bar: 300 nm). **b,** Eroded cervical dentin treated with NPs is shown after 7 d of storage (scale bar: 1 µm). Peritubular (PD) and intertubular dentin (ID) were strongly mineralized. A robust and rougher PD was observed (pointers). Dentinal tubules appeared partially filled with mineral precipitates (asterisks) and mineralized NPs (doubled arrows) (inset scale bar: 100 nm). A dense network of fibrils completely mineralized may be observed covering the peritubular dentin (arrows). The prototypical D-periodicity banding of collagen fibrils was observed in multiple details (faced arrows). **c,** Eroded cervical dentin treated with D-NPs is shown after 7 d of storage (scale bar: 3 µm). Dentinal tubules were empty. Intertubular (ID) and peritubular (PD) dentin were strongly mineralized (asterisks). At PD, mineral formed a lip around each tubule lumen detected. Mineralized collagen fibers and NPs formed the tubular wall (pointers). Crystal formations permit the observation of the subjacent collagen fibers which appeared clearly remineralized (arrows) (inset scale bar: 300 nm). **d,** Eroded cervical dentin surfaces treated with Ca-NPs are shown after

7 d of storage (scale bar: 1 μm). The dentin surface exhibited amorphous clumps of minerals scattered and grouped as dense network of buttons-like materials. Tubule entrances were visible. Peritubular (PD) and intertubular dentin (ID) appeared totally remineralized. Dentin collagen fibrils were coated with nucleated crystals (pointers). Dentinal tubules appeared partially filled with mineral precipitates (asterisks) and NPs (arrows) (inset scale bar: 300 nm). NPs remained totally adhered to the remineralized collagen fibers (faced arrows). **e**, Eroded dentin surfaces treated with Zn-NPs after 7 d of storage (scale bar: 2 μm). Tubules were not observed. Mineral precipitated throughout the dense network of multilayered crystals on the dentin surface were shown (arrows). Mineralized collagen fibrils were not noticeable below this coat of new crystals (inset scale bar: 300 nm). **f**, Spectra from energy dispersive analysis is showing elemental composition of phosphorous (P) and calcium (Ca), as main components in untreated (I), NPs (II), D-NPs (III), Ca-NPs (IV), and Zn-NPs (V) specimens of eroded cervical dentin

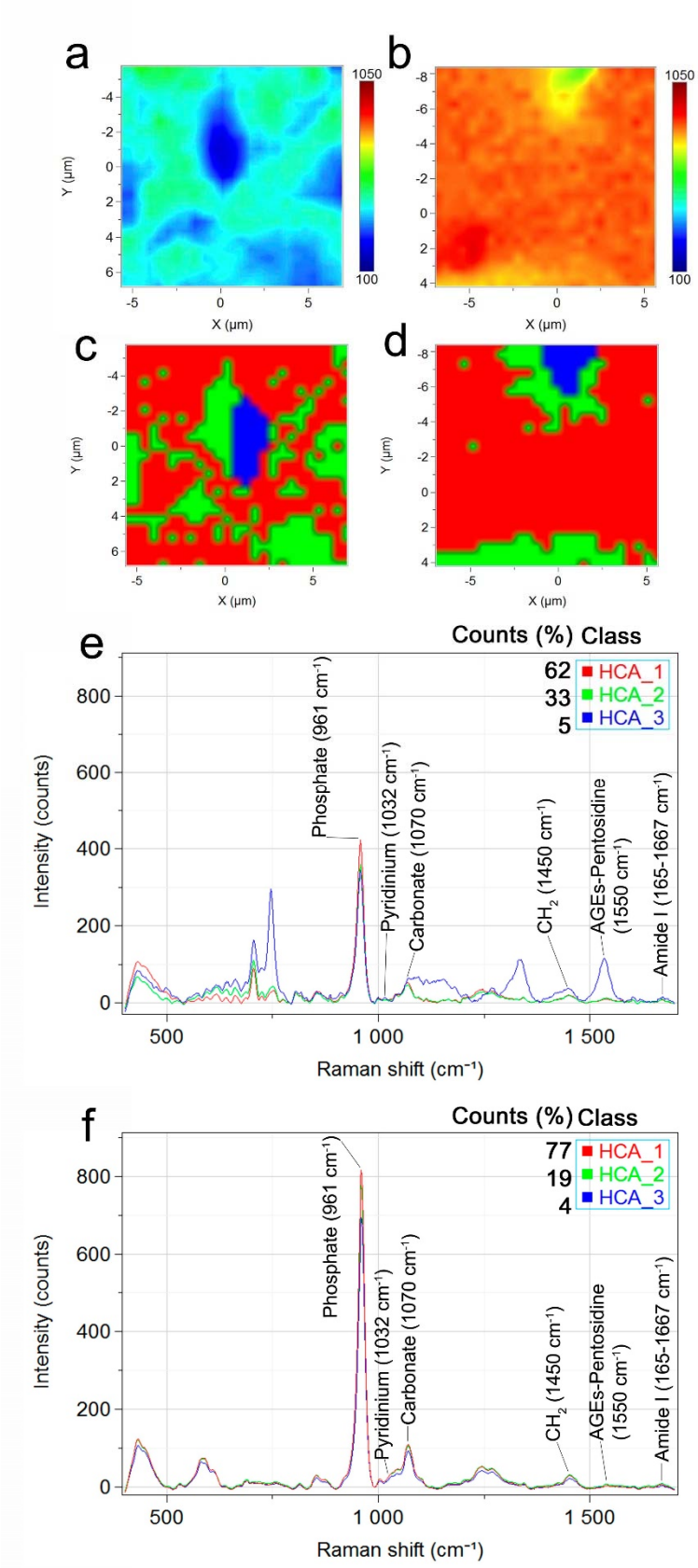

Fig 5 a, 2D micro-Raman map of the phosphate peak (961 cm^{-1}) intensities at the untreated surfaces, at 7 d of storage. **b,** 2D micro-Raman map of the phosphate peak (961 cm^{-1}) intensities at dentin surfaces treated with Zn-NPs, at 7 d of storage. **c,** Color mapping from hierarchical cluster analysis (HCA) image corresponding to the untreated surfaces, at 7 d of storage. **d,** Color mapping from hierarchical cluster analysis (HCA) image corresponding to dentin surfaces treated

with Zn-NPs, at 7 d of storage. Three levels of HCA clustering are shown. Areas of distinct colors have differences in Raman spectral distribution and chemical composition. Each cluster, corresponds to a different dentin location, which is assigned to a different color (red, green and blue). **e**, Raman spectra from hierarchical cluster analysis (HCA) results of untreated surfaces at 7 days of storage. **f,** Raman spectra from hierarchical cluster analysis (HCA) results of dentin surfaces treated with Zn-NPs at 7 d of storage.